Grasp Optimization under Specific Contact Constraints

Carlos Rosales, Josep M. Porta, and Lluís Ros.

***Abstract*—This paper presents a procedure to synthesize high-quality grasps for objects that need to be held and manipulated in a specific way, characterized by a pre-specified set of contact constraints to be satisfied. Due to the multi-modal nature of typical grasp quality measures, approaches that resort to local optimization methods are likely to get trapped into local extrema on such problem. An additional difficulty of the problem is that the set of feasible grasps is a highly-dimensional manifold, implicitly defined by a system of non-linear equations. The proposed procedure finds a way around these issues by focusing the exploration on a relevant subset of grasps of lower dimension, and tracing this subset exhaustively using a higher-dimensional continuation technique. A detailed atlas of the subset is obtained as a result, on which the highest-quality grasp according to any desired criterion, or a combination of criteria, can be readily identified. Examples are included that illustrate the application of the method to a three-fingered planar hand and to the Schunk anthropomorphic hand grasping several objects, using several quality indices.**

***Index Terms*—Grasp synthesis, precision grasp, grasp planning, contact constraint, anthropomorphic hand, grasp quality index.**

I. Introduction

MANY of the objects and tools used on everyday activities are designed to be grasped and manipulated in particular ways, determined by a given set of tight contact constraints between the hand and the object or tool. Consider, for instance, how a pen, a pair of scissors, or a jeweler's screwdriver are held, to properly write, cut a paper, or turn a screw, respectively. To perform these tasks with a robotic hand, we need to determine a suitable grasp for the object, i.e., a configuration of the hand in contact with the object at specific regions, allowing the manipulation to properly occur. This is the so-called grasp synthesis problem, which involves several subproblems [1]–[3]. The synthesized grasp must not only satisfy the required contact constraints avoiding undesired contacts [4]–[8]; it must also be force-closed to resist arbitrary force disturbances on the object [2, 9], manipulable to be able to move the object along any direction [10, 11], and as far as possible from losing these properties (Fig. 1). In general, thus, the generation of optimal grasps for precision tasks has to take several quality indices into account, either general (such as those related to force-closure or manipulability) or particular to the task to be performed [12, 13]. Some indices may even be conflicting, thus making their simultaneous consideration a challenging task, which justifies why most previous works focus on optimizing the grasp under a single criterion.

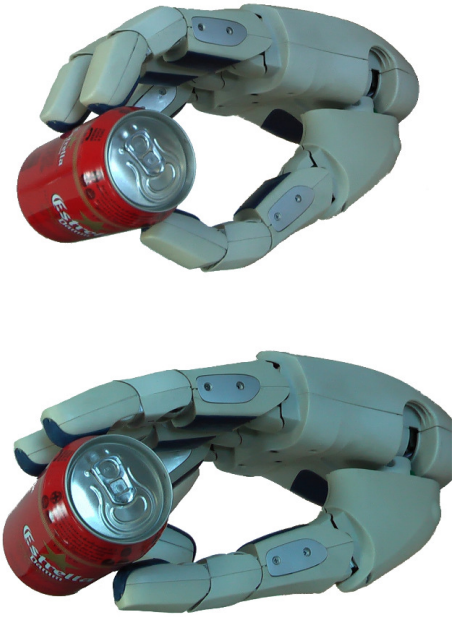

Fig. 1. Two grasps of a can for drink service. While both grasps are force-closed and manipulable, the top grasp is preferable. The fingers are almost fully extended in the bottom grasp, limiting the possibility to move the can in one direction.

Early approaches to the problem concentrate on the analysis of whether a given set of contact points on an object would yield a force-closed grasp [14, 15], or on determining contact regions on the object such that the force-closure property is guaranteed [16]–[22], but always neglecting the kinematic constraints imposed by the structure of the hand. As a consequence, the utility of such approaches is limited in practice, because the selected contact points or regions may not be reachable by the particular hand employed, once the object has to be grasped.

Recently, a more comprehensive approach to the problem has been attempted, which emphasizes the role of the kinematic constraints from the very beginning when searching for an optimal grasp [23]. The main difficulty in this case is that the set of hand configurations in contact with the object is a complex manifold, implicitly defined by a system of non-linear equations that express all joint-assembly and contact constraints involved in the hand-object system. To avoid this complexity, Ciocarlie and Allen [23] initially relax the contact

This work has been partially supported by the Spanish Ministry of Economy under contract DPI2010-18449.

The authors are with the Institut de Robòtica i Informàtica Industrial CSIC-UPC, Llorens i Artigas 4-6, Barcelona 08028, Spain (email: crosales@iri.upc.edu; porta@iri.upc.edu; ros@iri.upc.edu).

C. Rosales is also with the Institut d'Organització i Control de Sistemes Industrials (IOC), Diagonal 647, Barcelona 08028, Spain.

constraints, resulting in a search space that coincides with the configuration space of the hand. Typically, this space is of a high dimension, but principal hand motions [24] can be taken into account to narrow the search to a lower-dimensional subspace, which can be explored in reasonable times using simulated annealing. The hand configurations obtained, however, are not exactly in contact with the object and, thus, they must be evaluated with pre-grasp quality indices. Unfortunately, a good pre-grasp does not always result in a high-quality grasp, once the contact with the object is finally enforced through local techniques. The final hand-object contacts, moreover, may not be adequate to perform a given task and, hence, the technique is nicely suited to generate random grasps able to hold an object, but not those grasps allowing a particular manipulation of the object.

To generate a grasp fulfilling a specific set of contact constraints, both the joint-assembly constraints of the hand and the given contact constraints need to be enforced simultaneously, either using local search methods [4, 25] or global ones [8]. While the former are computationally less demanding, the latter can deal with more general types of contact constraints and guarantee to find a solution whenever one exists. Regardless of the adopted method, however, the returned grasp is not optimized in terms of any quality criterion, so that a final optimization process is needed to obtain a suitable high-quality grasp. Implementing such a process is not trivial though, since trying to optimize the grasp in a generate-and-test fashion is computationally too expensive. Moreover, local optimization methods [26] are likely to get trapped into local optima, because, except in simple cases [27, 28], grasp quality indices present local extrema.

This paper integrates different techniques to produce a novel grasp optimization procedure that circumvents the problems of existing approaches. The procedure entails characterizing the manifold of feasible grasps by a system of equations (Section II), then extending this system with meaningful equations to reduce the dimension of its solution set (Section III), and finally performing an exhaustive search over a point grid discretizing such set at a desired resolution, to determine the highest-quality grasp attainable on the grid (Section IV). The grid is derived by resorting to recently-developed techniques for higher-dimensional continuation [29], which are able to compute exhaustive representations of implicitly-defined manifolds of moderate dimensions in reasonable times. The procedure is very general and applicable to virtually any relevant hand and object geometry, and it can be used under any quality criterion or a combination of criteria, because it only requires the evaluation of the quality function on selected points, without making particular assumptions on the mathematical properties of the function. The approach extends the one preliminarily presented in [30] in that it assumes a more general contact model, and the possibility to account for several quality criteria simultaneously. Test cases are provided that validate the approach on simple and complex robotic hands grasping objects with different geometries, under typical force-closure and manipulability indices (Section V).

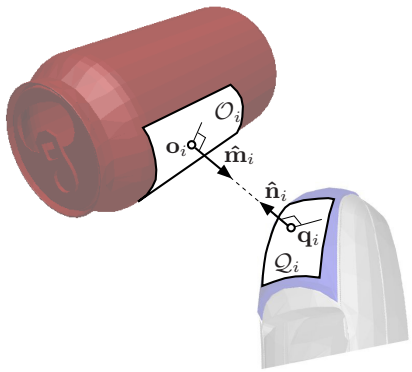

Fig. 2. Elements intervening in the i-th contact constraint. Points $\mathbf{q}_i \in \mathcal{Q}_i$ and $\mathbf{o}_i \in \mathcal{O}_i$ must coincide, with the normals $\hat{\mathbf{n}}_i$ and $\hat{\mathbf{m}}_i$, aligned, to avoid local hand-object inter-penetrations.

II. Feasible Grasps

In this work, a feasible grasp is assumed to be a configuration of the hand-object system in which a number of regions of the hand $\mathcal{Q}_i$, $i = 1, \ldots, m$, are in contact with corresponding regions $\mathcal{O}_i$ on the object. The regions and their pairings are pre-specified, and the contact between $\mathcal{Q}_i$ and $\mathcal{O}_i$ is assumed to be established with a point $\mathbf{q}_i \in \mathcal{Q}_i$ coinciding with another point $\mathbf{o}_i \in \mathcal{O}_i$, keeping aligned the surface normals at such points, $\hat{\mathbf{n}}_i$ and $\hat{\mathbf{m}}_i$, to avoid local hand-object inter-penetrations (Fig. 2). We further assume that the hand joints are independently actuated or mechanically coupled, but do not consider the case of adaptive underactuated hands [31].

Following [8], a grasp configuration can be represented by a vector $\mathbf{x} = (\mathbf{x}_\mathrm{h}^\top, \mathbf{x}_\mathrm{o}^\top, \mathbf{x}_\mathrm{c}^\top)^\top \in \mathbb{R}^n$ of generalized coordinates, where $\mathbf{x}_\mathrm{h}$ and $\mathbf{x}_\mathrm{o}$ determine the configuration of the hand and the object, respectively, and $\mathbf{x}_\mathrm{c}$ encompass contact-related coordinates. The vector $\mathbf{x}$ defines a feasible grasp if it satisfies the following equations. A first set of equations,

$$\mathbf{H}(\mathbf{x}_\mathrm{h}) = \mathbf{0}, \tag{1}$$

enforces $\mathbf{x}_\mathrm{h}$ to be a valid hand configuration, i.e., one respecting the assembly constraints imposed by the joints (usually revolute or universal) on the various bodies they connect (the palm and the several finger phalanges). Note that Eq. (1) is not necessary if the coordinates in $\mathbf{x}_\mathrm{h}$ are independent, as it happens for instance when choosing joint angles to represent a configuration [32]. In our case, however, we resort to the dependent coordinates defined in [33] because they yield equations of simple structure, which has proved beneficial in the context of grasp synthesis [8], and for the application of continuation techniques [34]. In particular, this formulation encodes the spatial pose of each body of the hand with twelve variables, providing the position vector and the rotation matrix of a local reference frame attached to the body, relative to an absolute frame attached to the palm. Thus, in addition to including the joint assembly constraints, Eq. (1) includes constraints to enforce the twelve pose variables of each body to define a member of $SE(3)$. Similarly, the spatial pose of the object is encoded by twelve variables, so that a second set of equations,

$$\mathbf{L}(\mathbf{x}_\mathrm{o}) = \mathbf{0}, \tag{2}$$

constrains $\mathbf{x}_\mathrm{o}$ to define a member of $SE(3)$. A last set of equations, finally, enforces the contact constraints between the hand and the object. To this end, we assume that each contact region $\mathcal{Q}_i$ is specified as a regular parametrized patch, i.e., as a smooth function of the form

$$\mathbf{q}_i = \mathbf{Q}_i(s_i, t_i, \mathbf{x}_\mathrm{h}), \tag{3}$$

providing the absolute coordinates of a point $\mathbf{q}_i = (x_i, y_i, z_i)$ in the patch as a function of two patch parameters s_i and t_i, and of the hand configuration $\mathbf{x}_\mathrm{h}$. Analogously, the normal to any point in this patch is assumed to be given by a smooth function

$$\hat{\mathbf{n}}_i = \mathbf{N}_i(s_i, t_i, \mathbf{x}_\mathrm{h}). \tag{4}$$

In general, Eqs. (3) and (4) define two-dimensional regions described, for example, by Bézier patches [35], but they can be replaced by single-parameter curves or fixed points if desired. The points and normals on the $\mathcal{O}_i$ patches are similarly defined as a function of two patch parameters u_i and v_i, and of the object pose $\mathbf{x}_\mathrm{o}$, through expressions of the form

$$\mathbf{o}_i = \mathbf{O}_i(u_i, v_i, \mathbf{x}_\mathrm{o}), \tag{5}$$

$$\hat{\mathbf{m}}_i = \mathbf{M}_i(u_i, v_i, \mathbf{x}_\mathrm{o}), \tag{6}$$

so that the contact of $\mathcal{Q}_i$ with $\mathcal{O}_i$ can be enforced by setting

$$\mathbf{q}_i - \mathbf{o}_i = \mathbf{0}, \tag{7}$$

$$\hat{\mathbf{n}}_i + \hat{\mathbf{m}}_i = \mathbf{0}. \tag{8}$$

Thus, the vector $\mathbf{x}_\mathrm{c}$ encompasses the vectors $\mathbf{q}_i$, $\hat{\mathbf{n}}_i$, $\mathbf{o}_i$, and $\hat{\mathbf{m}}_i$, and the patch parameters s_i, t_i, u_i, and v_i intervening in Eqs. (3)-(8), for $i = 1, \ldots, m$.

Each variable in $\mathbf{x} = (\mathbf{x}_\mathrm{h}^\top, \mathbf{x}_\mathrm{o}^\top, \mathbf{x}_\mathrm{c}^\top)^\top$ can only take values within a given range. For instance, the variables defining the orientation matrices in $\mathbf{x}_\mathrm{h}$ and $\mathbf{x}_\mathrm{o}$ take values within $[-1, 1]$. Also, the size of the hand provides interval bounds on the translation variables, and, without loss of generality, the patch parameters of the contact regions can be normalized to the $[0, 1]$ range [35]. Thus, the Cartesian product of such ranges defines a rectangular domain $\mathcal{D} \subset \mathbb{R}^n$ where the search for an optimal feasible grasp is to be confined.

In sum, the set of feasible grasps $\mathcal{F}$ encompasses the points $\mathbf{x} \in \mathcal{D}$ satisfying the system

$$\mathbf{F}(\mathbf{x}) = \mathbf{0} \tag{9}$$

formed by Eqs. (1) and (2), and Eqs. (3)-(8) for all contacts $i = 1, \ldots, m$. The formulation in [8] guarantees that $\mathbf{F}(\mathbf{x})$ is differentiable and, to keep the presentation of the method as simple as possible, we assume that its Jacobian is full rank for all $\mathbf{x} \in \mathcal{F}$, which is the generic situation according to Sard's theorem of Analysis. Thus, $\mathcal{F}$ can be assumed to be a smooth manifold of dimension $t = n - f$, where f is the number of scalar equations in (9).

Using Eq. (9), the method in [8] can now be applied to determine an initial grasp $\mathbf{x}_1 \in \mathcal{F}$ from which to start the search for an optimal grasp in $\mathcal{F}$. However, we emphasize that other grasp synthesis techniques could also be used to compute $\mathbf{x}_1$ [4, 25], because the method in this paper makes no assumption on how this configuration is obtained.

III. Relevant grasps

Although obtaining points on $\mathcal{F}$ is feasible, the dimension of this space is very large in practice, which hinders its exhaustive exploration independently of the methodology adopted. In the context of grasping, however, studies on the human behavior suggest that humans do not use all degrees of freedom of the hand independently, but in a coordinated way [24]. Following this idea, anthropomorphic hands are usually controlled using principal hand motions (also called hand postural synergies [24, 36], eigengrasps [23], or principal motion directions [37]), where few coordinated motions are used to account for the overall motion capability of the hand. By taking principal hand motions into consideration, the search of a good grasp can be narrowed to a subset of relevant grasps $\mathcal{R} \subset \mathcal{F}$ of lower dimension, thus speeding up the overall optimization process.

Principal hand motions are computed via linear dimension-reduction techniques on a representative set of hand configurations $\mathbf{X}_\mathrm{h} = \{\mathbf{x}_\mathrm{h}^1, \ldots, \mathbf{x}_\mathrm{h}^z\}$, where each $\mathbf{x}_\mathrm{h}^i$ is a value of $\mathbf{x}_\mathrm{h}$ satisfying Eq. (1). Let h be the number of components in $\mathbf{x}_\mathrm{h}$, $\bar{\mathbf{x}}_\mathrm{h}$ the average of the configurations in $\mathbf{X}_\mathrm{h}$, and $\mathbf{T}$ an $h \times z$ matrix whose i-th column is $\mathbf{x}_\mathrm{h}^i - \bar{\mathbf{x}}_\mathrm{h}$. The principal component analysis of $\mathbf{X}_\mathrm{h}$ can be performed by diagonalizing the covariance of $\mathbf{T}$,

$$\mathbf{T}\,\mathbf{T}^\top = \mathbf{E}\,\mathbf{S}^2\,\mathbf{E}^\top.$$

The $h \times h$ orthonormal matrix $\mathbf{E}$ gives the directions of variance of the data, and the diagonal matrix $\mathbf{S}^2$ is the variance in each one of these directions, sorted in decreasing magnitude. The linear variety through $\bar{\mathbf{x}}_\mathrm{h}$ generated by the first p columns of $\mathbf{E}$ defines the set $\mathcal{E}$ of the p principal hand motions. The vectors in $\mathcal{E}$ have null components along the columns of $\mathbf{E}_s$, the matrix formed by the last $s = h - p$ columns of $\mathbf{E}$, so that $\mathcal{E}$ is the solution set of

$$\mathbf{E}_s^\top(\mathbf{x}_\mathrm{h} - \bar{\mathbf{x}}_\mathrm{h}) = \mathbf{0}. \tag{10}$$

This equation, together with (9), defines the system

$$\mathbf{R}(\mathbf{x}) = \mathbf{0}, \tag{11}$$

characterizing the non-linear set $\mathcal{R} = \mathcal{F} \cap \mathcal{E}$ of relevant grasps. In the generic case, the Jacobian of $\mathbf{R}(\mathbf{x})$ will also be full rank for all $\mathbf{x} \in \mathcal{R}$, so that, like $\mathcal{F}$, $\mathcal{R}$ can also be assumed to be a smooth manifold with no bifurcations, which allows adopting a simplified continuation strategy below, with no provisions for branch switching operations [38].

Since t is the dimension of $\mathcal{F}$, and k is the desired dimension for $\mathcal{R}$, then we must set

$$s = t - k. \tag{12}$$

For efficiency reasons, k must be small in the adopted continuation method (typically below 5), and s must be set accordingly. However, s must be smaller than h, which limits the amount of dimension reduction obtained by the use of principal hand motions. As we will see, however, this is not an issue in practice, since the amount of dimension reduction to be introduced is moderate in all cases, due to the presence of the contact constraints. Actually, these constraints allow

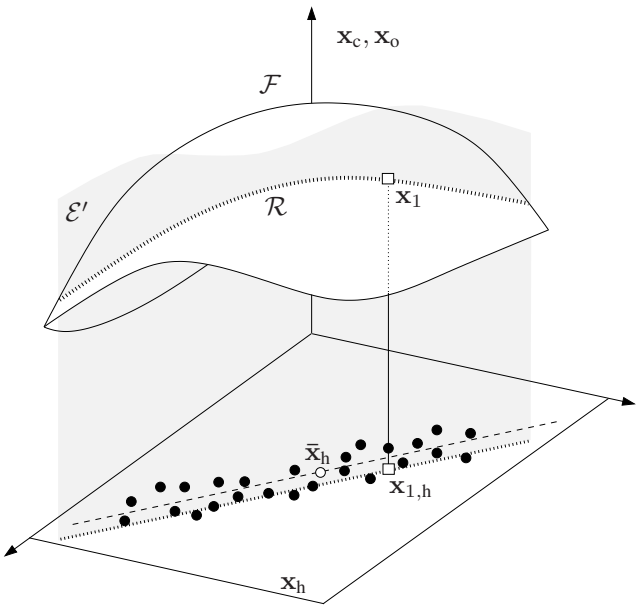

Fig. 3. Schematic representation of the spaces involved in the optimization framework presented in this paper. See the text for details.

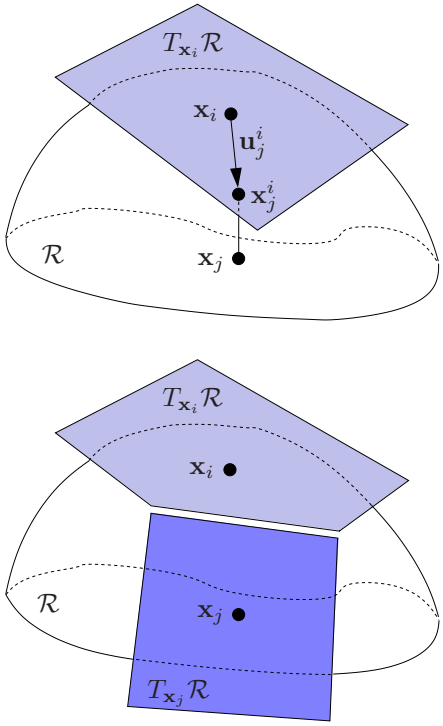

Fig. 4. The higher-dimensional continuation method applied to a two-dimensional manifold $\mathcal{R}$ in 3D space. Using the chart centered at $\mathbf{x}_i$, a point $\mathbf{x}_j^i$ on the chart corresponding to a vector $\mathbf{u}_j^i \in T_{\mathbf{x}_i}\mathcal{R}$ is orthogonally projected to obtain a point $\mathbf{x}_j \in \mathcal{R}$ (top). If a new chart is defined at $\mathbf{x}_j$, it must be properly coordinated with the chart at $\mathbf{x}_i$ so that their projections smoothly cover the manifold (bottom).

using a significantly smaller s (i.e., a larger p) than that used in existing approaches relying on principal hand motions.

Nonetheless, the introduction of principal hand motions might lead to an empty set $\mathcal{R}$ if the contact points are not reachable by the hand when constrained to be in $\mathcal{E}$. To guarantee that $\mathcal{R}$ is not empty, this set is redefined as $\mathcal{R} = \mathcal{F} \cap \mathcal{E}'$ hereafter, where $\mathcal{E}'$ is the solution set of

$$\mathbf{E}_s^\top (\mathbf{x}_\mathrm{h} - \mathbf{x}_{1,\mathrm{h}}) = \mathbf{0}, \tag{13}$$

with $\mathbf{x}_{1,\mathrm{h}}$ being the subvector of the initial grasp $\mathbf{x}_1$ containing the values of $\mathbf{x}_\mathrm{h}$. In general, the difference of using Eq. (13) instead of Eq. (10) is minor, since $\mathbf{x}_{1,\mathrm{h}}$ is usually close to the original set of principal hand motions, but this approximation ensures that the hand can always conform to the object surface because $\mathcal{R}$ will at least include the initial feasible grasp $\mathbf{x}_1$.

Fig. 3 summarizes the different elements involved in the approach. $\mathcal{F}$ is the set of feasible grasps defined in the space of $\mathbf{x}_\mathrm{h}$, $\mathbf{x}_\mathrm{o}$, and $\mathbf{x}_\mathrm{c}$. In this representation, the configurations in $\mathbf{X}_\mathrm{h}$ are shown as black dots, the white dot is their average, $\bar{\mathbf{x}}_\mathrm{h}$, and the original set of p principal hand motions is shown as a dashed line in the $\mathbf{x}_\mathrm{h}$ plane. The latter set is approximated by a line through $\mathbf{x}_{1,\mathrm{h}}$, shown dotted in the figure, which, when extended to the whole space, generates the linear variety $\mathcal{E}'$. Finally, the set $\mathcal{R} = \mathcal{F} \cap \mathcal{E}'$ is the space where the grasp optimization is to be performed. Note that $\mathcal{R}$ is one-dimensional in this schematic representation, but it is a k-dimensional set in general.

Typically, previous methods that use principal hand motions explore $\mathcal{E}$. Then, they try to modify points on such space to yield configurations in contact with the object using local methods,. However, the final configurations may not necessarily lie on the set $\mathcal{F}$ of grasps satisfying the contact constraints required for the task. In contrast, our method directly operates on the set $\mathcal{R}$, which is fully included in $\mathcal{F}$.

IV. Grasp Quality Optimization

In this paper, the search for an optimal grasp is performed by computing an atlas of the k-dimensional manifold $\mathcal{R}$ just defined, including the relevant grasps. Such an atlas provides a collection of charts, where each chart parametrizes a portion of $\mathcal{R}$, and this allows enumerating a representative collection of grasps in $\mathcal{R}$, on which any quality index can be evaluated to detect the optimal one.

A. Tracing the Manifold of Relevant Grasps

Formally, a chart $\mathcal{C}_i$ is a local map from a parameter domain $\mathcal{P}_i \subset \mathbb{R}^k$ to an open neighborhood around a given point $\mathbf{x}_i \in \mathcal{R}$, initially $\mathbf{x}_1$. The higher-dimensional continuation method proposed in [39] defines the map for chart $\mathcal{C}_i$ using $\mathbf{\Phi}_i$, an $n \times k$ orthonormal basis of $T_{\mathbf{x}_i}\mathcal{R}$, the k-dimensional tangent space of $\mathcal{R}$ at $\mathbf{x}_i$. The map is constructed by first selecting a k-dimensional vector of parameters $\mathbf{u}_j^i \in T_{\mathbf{x}_i}\mathcal{R}$ (Fig. 4, top), and then using this vector to generate a point $\mathbf{x}_j^i \in \mathbb{R}^n$ in the neighborhood of $\mathbf{x}_i$ using

$$\mathbf{x}_j^i = \mathbf{x}_i + \mathbf{\Phi}_i \, \mathbf{u}_j^i. \tag{14}$$

Then, the point $\mathbf{x}_j \in \mathcal{R}$ that corresponds to the orthogonal projection of $\mathbf{x}_j^i$ on $\mathcal{R}$ is computed, by solving the system

$$\left.\begin{aligned} \mathbf{R}(\mathbf{x}_j) &= \mathbf{0} \\ \mathbf{\Phi}^\top (\mathbf{x}_j - \mathbf{x}_j^i) &= \mathbf{0} \end{aligned}\right\}, \tag{15}$$

using a Newton-Raphson method initialized at $\mathbf{x}_j^i$.

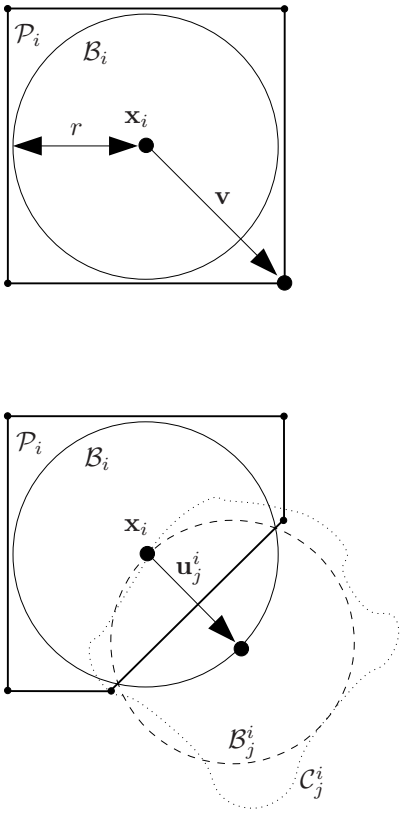

Fig. 5. The process of chart construction. The domain $\mathcal{P}_i$ of chart $\mathcal{C}_i$ is initialized as a box in $T_{\mathbf{x}_i}\mathcal{R}$ circumscribing a ball of radius r centered in $\mathbf{x}_i$ (top). $\mathcal{P}_i$ is refined using a ball $\mathcal{B}_j^i$ that approximates $\mathcal{C}_j^i$, the projection on $\mathcal{C}_i$ of the part of the manifold covered by $\mathcal{C}_j$ (bottom).

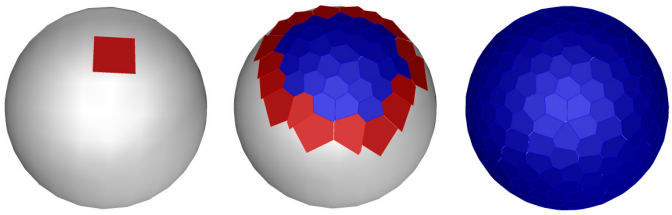

Fig. 6. Three stages in the construction of an atlas over a sphere. Red and blue polygons represent charts under expansion and charts whose domain is already bounded, respectively.

Each point on the manifold is the potential center of a new chart (Fig. 4, bottom), and the method introduced by Henderson [39] can be used to select the chart centers, in order to define an atlas with a good coverage of the manifold. Using this approach, the domain $\mathcal{P}_i$ of a chart $\mathcal{C}_i$ is initialized as a k-dimensional hypercube enclosing a ball $\mathcal{B}_i$ of radius r, where $\mathcal{P}_i$ and $\mathcal{B}_i$ are both defined in $T_{\mathbf{x}_i}\mathcal{R}$ as illustrated in Fig. 5 (top). A vertex of $\mathcal{P}_i$ exterior to $\mathcal{B}_i$, with position vector $\mathbf{v}$, is then employed to generate a point $\mathbf{x}_j^i$, using Eq. (14) with

$$\mathbf{u}_j^i = \frac{\alpha}{\|\mathbf{v}\|}\,\mathbf{v}, \tag{16}$$

where α is initialized to r. If the projection of $\mathbf{x}_j^i$ on $\mathcal{R}$ does not converge, or if the new chart $\mathcal{C}_j$ at $\mathbf{x}_j$ is too far or too

Algorithm 1: Computation of the atlas of $\mathcal{R}$

AtlasComputation($\mathbf{F}, \mathbf{X}_\text{h}, \mathbf{x}_1, t, k, r, \epsilon$)
input : The set $\mathbf{F}$ of equations , the set $\mathbf{X}_\text{h}$ of representative hand configurations, the initial grasp $\mathbf{x}_1$, the dimension t of $\mathcal{F}$, the desired dimension k for $\mathcal{R}$, and the parameters r and ϵ used to build the atlas.
output: An atlas $\mathcal{A}$ of $\mathcal{R}$.

$\mathbf{E} \leftarrow$ PRINCIPALHANDMOTIONS($\mathbf{X}_\text{h}$)
$s \leftarrow t - k$
$\mathbf{R} \leftarrow \mathbf{F} \cup \{\mathbf{E}_s(\mathbf{x}_\text{h} - \mathbf{x}_{1,\text{h}})\}$
$\mathcal{A} \leftarrow \{$GENERATECHART($\mathbf{R}, \mathbf{x}_1, r$)$\}$
while not BOUNDED($\mathcal{A}$) **do**
  $\mathcal{C}_i \leftarrow$NOTBOUNDEDCHART($\mathcal{A}$)
  $\alpha \leftarrow r$
  $\mathbf{v} \leftarrow$EXPANDIBLEVERTEX($\mathcal{C}_i$)
  repeat
    $\mathcal{C}_j \leftarrow$NEWCHART($\mathbf{R}, \mathcal{C}_i, \alpha, \mathbf{v}, r$)
    $\alpha \leftarrow \alpha \cdot 0.9$
  until SIMILARCHARTS($\mathcal{C}_i, \mathcal{C}_j, \epsilon$)
  $\mathcal{A} \leftarrow \mathcal{A} \cup \{\mathcal{C}_j\}$
RETURN($\mathcal{A}$)

different from $\mathcal{C}_i$, i.e., if

$$\|\mathbf{x}_j - \mathbf{x}_j^i\| > \epsilon, \tag{17}$$

or

$$\|\mathbf{\Phi}_i^\top \mathbf{\Phi}_j\| < 1 - \epsilon, \tag{18}$$

for a given threshold ϵ, then the new chart is discarded and a new attempt of chart generation is performed with a smaller α. This procedure adapts the size of the domain for each chart to the local curvature of the manifold. When $\mathcal{C}_j$ is valid, it is used to refine $\mathcal{P}_i$ from the intersection between $\mathcal{B}_i$ and $\mathcal{C}_j^i$, the projection on $T_{\mathbf{x}_i}\mathcal{R}$ of the part of the manifold covered by $\mathcal{C}_j$. This projection is approximated by a ball $\mathcal{B}_j^i$ in $T_{\mathbf{x}_i}\mathcal{R}$, as shown in Fig. 5 (bottom). The intersection of $\mathcal{B}_i$ and $\mathcal{B}_j^i$ defines a new face of $\mathcal{P}_i$ that eliminates some of its vertices (in particular the one given by $\mathbf{v}$) and generates new ones. Similarly, the polytope $\mathcal{P}_j$ associated with $\mathcal{C}_j$ is cropped using the projection of $\mathcal{C}_i$ on $\mathcal{C}_j$. The previous process can be iterated and, when all vertices of $\mathcal{P}_i$ are included in $\mathcal{B}_i$, the chart is said to be bounded. Moreover, charts whose center is out of the domain $\mathcal{D}$ defined in Section II are also considered bounded. If $\mathcal{R}$ has the manifold structure everywhere and r is properly set [39], then when all charts are bounded, the atlas fully covers the connected component of $\mathcal{R}$ containing the initial point $\mathbf{x}_1$ (Fig. 6).

Algorithm 1 summarizes the atlas computation procedure. The algorithm receives as inputs the set $\mathbf{F}$ of equations implicitly defining $\mathcal{F}$, the set $\mathbf{X}_\text{h}$ of representative hand configurations, the initial grasp $\mathbf{x}_1$, the dimension t of $\mathcal{F}$, the desired dimension k for $\mathcal{R}$, and the parameters r and ϵ used to construct the atlas. As output, the algorithm returns an atlas $\mathcal{A}$ of the component of $\mathcal{R}$ reachable from $\mathbf{x}_1$. The algorithm determines the principal hand motions as described

Algorithm 2: The grasp optimization process.

GraspOptimization($\mathcal{A}, d, \mathbf{I}, \mathbf{l}, \mathbf{w}$)
input : The atlas $\mathcal{A}$, the number d of points to consider on each chart, the set $\mathbf{I}$ of quality measures to be optimized, and the vectors $\mathbf{l}$ and $\mathbf{w}$ of lower bounds and weights for the quality measures, respectively.
output: The optimal grasp $\mathbf{x}_g$.

1 $g \leftarrow -\infty$
2 $\mathbf{x}_g \leftarrow \varnothing$
3 **forall** $\mathcal{C} \in \mathcal{A}$ **do**
4 $\quad \mathcal{U} \leftarrow$ POINTSONCHART($\mathcal{C}, d$)
5 $\quad$ **forall** $\mathbf{u} \in \mathcal{U}$ **do**
6 $\quad\quad \mathbf{x} \leftarrow$ CHARTTOMANIFOLD($\mathcal{C}, \mathbf{u}$)
7 $\quad\quad \mathbf{q} \leftarrow \mathbf{I}(\mathbf{x})$
8 $\quad\quad$ **if** $\mathbf{q} \succeq \mathbf{l}$ **then**
9 $\quad\quad\quad q \leftarrow \mathbf{w}^T\mathbf{q}$
10 $\quad\quad\quad$ **if** $q \geq g$ **then**
11 $\quad\quad\quad\quad \mathbf{x}_g \leftarrow \mathbf{x}$
12 $\quad\quad\quad\quad g \leftarrow q$
13 RETURN($\mathbf{x}_g$)

in Section III (line 1). The required number of constraints relative to such motions is then computed as a function of t and k (line 2) in order to obtain the set $\mathbf{R}$ of equations defining $\mathcal{R}$ (line 3). Then, $\mathcal{A}$ is initialized with a chart centered in $\mathbf{x}_1$ (line 4), and the construction of $\mathcal{A}$ proceeds while any of the charts can be extended (lines 5 to 13). The extension of a chart $\mathcal{C}_i$ starts by selecting a vertex of $\mathcal{P}_i$ not included in $\mathcal{B}_i$ (line 8). This vertex is used to generate a new chart $\mathcal{C}_j$ (line 10) using Eqs. (14) to (16) to determine its center. If the difference between the new chart and the previous one is too large according to Eqs. (17) and (18), chart generation is attempted closer to $\mathbf{x}_i$, i.e., with a smaller α (line 11). Otherwise, the new chart is added to $\mathcal{A}$, coordinating the chart with those already included in $\mathcal{A}$ (line 13). The computational cost of this algorithm is exponential in k and, therefore, it is only practical to compute the atlas on manifolds of moderate dimension, typically below 5. The larger the number of principal hand motions considered –i.e., the smaller s in Eq. (10)–, the larger the amount of motion capability of the hand taken into account, but also the higher the value of k. Thus, a trade off must be reached to include enough principal hand motions in the problem without having a too large k. As we will see in the experiments, a small k can be obtained by neglecting a minimum of the motion capabilities captured in the set of hand configurations $\mathbf{X}_\mathrm{h}$.

B. Evaluating the Quality of Relevant Grasps

Once the atlas is computed, we can identify the optimal grasp over $\mathcal{R}$ by considering a set $\mathbf{I}$ of quality indices. Commonly, the quality indices are combined either in series or in parallel [40]. In the first case, only grasps with a minimum value for a given index are evaluated with the subsequent indices. In the second case, all indices are evaluated simultaneously and combined to produce a single measure, typically using a weighted sum after normalizing them. Algorithm 2 allows these two ways of combining the quality indices. The algorithm iterates over all charts in the atlas $\mathcal{A}$ (lines 3-12). For each chart $\mathcal{C}$ in $\mathcal{A}$, it generates a set $\mathcal{U}$ of d points on the tangent space associated with this chart (line 4). These points can be either computed on a regular grid or sampled randomly but, in any case, they all must lie inside the domain of $\mathcal{C}$. The number d of points to generate depends on the resolution at which the optimal grasp is required, and on the smoothness of the quality indices considered; i.e., the sharper the variations the denser the set of points. For each one of the points in $\mathcal{U}$, we obtain the corresponding point on $\mathcal{R}$ (line 6) using Eqs. (14) and (15). Then, for each point on $\mathcal{R}$ we evaluate the quality indices in $\mathbf{I}$ (line 7). If the obtained values for the indices are all above the required thresholds in an element-wise comparison (line 8), we combine the indices (line 9), and then check whether the combined value is larger than that of the best grasp found up to the moment (lines 10-12). By setting the appropriate thresholds in $\mathbf{l}$ and using $\mathbf{w} = (0, \ldots, 0, 1)^\top$ we will obtain a serial evaluation of the indices in which the last index in $\mathbf{I}$ will be optimized. A parallel evaluation can be obtained by using $\mathbf{l} = (-\infty, \ldots, -\infty)^\top$ and setting the desired values in $\mathbf{w}$. Mixed evaluation schemes can be obtained too, by adequately setting $\mathbf{l}$ and $\mathbf{w}$. By iterating over all charts and points, the optimal grasp over the computed points of $\mathcal{R}$ is finally identified and returned (line 13). In an extreme case, the algorithm could return no grasp if the quality indices for all of the considered grasps are below the given thresholds. The overall cost of this algorithm is bilinear with the number of charts in the atlas, and with the number d of points considered for each chart.

Note that, as long as the kinematic structure of the hand-object system remains constant, there is no need to recompute the atlas for every new index evaluation. This is specially relevant in distance-to-collision indices, which can be re-evaluated over the same atlas upon obstacle changes in the environment, provided that the object to be grasped and the contact regions continue to be the same. Moreover, if an optimal grasp is required with a finer precision, we only need to use Algorithm 2 with a larger value of d and, again, there is no need to recompute the atlas. In a multi-resolution optimization context, this refinement can be focused into the most promising areas previously identified.

V. TEST CASES

For the sake of clarity, we first exemplify the application of the optimization procedure on a simple hand, and then summarize the results for the Schunk anthropomorphic hand. All results correspond to an implementation in C of Algorithm 1, and in Matlab of Algorithm 2, both available in [41], executed on an Intel Core 2 Duo processor at 3 GHz.

A. A planar hand

Fig. 7 shows a planar hand with three fingers and two phalanges per finger holding an object composed of circles,

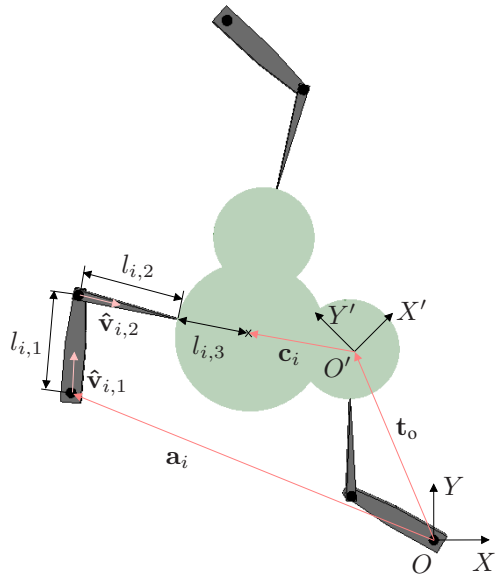

Fig. 7. A simple planar hand with three fingers holding an object. The parameters are indicated for one finger only, but apply to the three fingers.

where the OXY absolute reference frame is attached to the base of one of the fingers. The length and absolute orientation of the j-th phalanx of the i-th finger are given by the parameter $l_{i,j}$ and the unit vector $\hat{\mathbf{v}}_{i,j} \in \mathbb{R}^2$, respectively. Since the lengths are fixed, the configuration of the hand can be encoded in a simplified form in this case, by the vector $\mathbf{x}_h = (\hat{\mathbf{v}}_{1,1}^\top, \ldots, \hat{\mathbf{v}}_{3,2}^\top)^\top$ subject to the constraints

$$\|\hat{\mathbf{v}}_{i,j}\|^2 = 1, \tag{19}$$

for all phalanges. Thus, Eq. (1) is the system formed by Eqs. (19). Since this system contains 6 equations in 12 variables, its solution set is of dimension 6, which agrees with the number of degrees of freedom of the hand. Note that $\mathbf{x}_h$ only includes parameters for the orientation of the hand links, since their position vectors can be computed from the orientations and the constant length parameters [33].

A local reference frame $O'X'Y'$ is attached to the object, whose pose in the absolute frame is given by $\mathbf{x}_o = (\mathbf{t}_o, \hat{\mathbf{v}}_o)$, where $\mathbf{t}_o = (x_o, y_o)^\top$ is the position vector of O' and $\hat{\mathbf{v}}_o = (s_o, c_o)^\top$ is a unit vector aligned with the X' axis. Then, Eq. (2) becomes

$$\|\hat{\mathbf{v}}_o\|^2 = 1. \tag{20}$$

In this example, the contact regions in each fingertip reduce to a point and the explicit expression of Eq. (3) is

$$\mathbf{q}_i = \mathbf{a}_i + l_{i,1}\,\hat{\mathbf{v}}_{i,1} + l_{i,2}\,\hat{\mathbf{v}}_{i,2}, \tag{21}$$

where $\mathbf{a}_i$ is the position vector of the palm anchor point of finger i in the absolute frame, and Eq. (4) providing the associated normal is

$$\hat{\mathbf{n}}_i = \hat{\mathbf{v}}_{i,2}. \tag{22}$$

Moreover, the contact regions on the object are arcs of circumference given by a single parameter. Thus, for each one of such arcs, Eq. (5) boils down to the following expression

$$\mathbf{o}_i = \mathbf{t}_o + \begin{bmatrix} c_o & -s_o \\ s_o & c_o \end{bmatrix} (\,\mathbf{c}_i + l_{i,3}\,\hat{\mathbf{w}}(u_i)), \tag{23}$$

where $\mathbf{c}_i$ is the center of the circumference in local coordinates of the object, $l_{i,3}$ is its radius, and

$$\hat{\mathbf{w}}(u_i) = \begin{bmatrix} \cos u_i \\ \sin u_i \end{bmatrix}, \tag{24}$$

with $u_i \in [a_i, b_i]$, is the angular range defining the arc for contact patch i. Similarly, Eq. (6) reduces to

$$\hat{\mathbf{m}}_i = \begin{bmatrix} c_o & -s_o \\ s_o & c_o \end{bmatrix} \hat{\mathbf{w}}(u_i), \tag{25}$$

in this case. Thus, Eq. (9) encompasses Eqs. (19) to (25) together with Eqs. (7) and (8), defining a set $\mathcal{F}$ of feasible grasps of dimension $t = 3$. The proposed optimization procedure can be directly applied to problems of this dimension. However, to complete the example and to facilitate the visualization of the results, it is better to reduce the dimension to obtain a set of relevant grasps $\mathcal{R}$ of dimension $k = 2$. Thus, according to Eq. (12), $s = 1$ linear constraints given by Eq. (13) must be added to Eq. (9), in order to get Eq. (11). In this example, the set $\mathbf{X}_h$ used to reduce the dimensionality contains randomly generated hand configurations.

Fig. 8 shows the results obtained when applying the proposed method to this example. Two complementary views of the computed atlas are depicted (left), together with the best and worst grasps found (center and right, respectively). The atlas was obtained using Algorithm 1 with $r = 0.125$ and $\epsilon = 0.4$ in about 0.1 seconds. It contains a total of 750 charts, whose polytopes $\mathcal{P}_i$ form the shown hexagonal-like mesh. To optimize the grasp, the atlas was evaluated using Algorithm 2 under the force-closure quality index reported by Prattichizzo and Trinkle [2] normalized to the range $[0, 1]$, obtaining the results shown in Fig. 8, where green and red charts respectively correspond to configurations with a large and low value of the index. Thus, Algorithm 2 was called with $\mathbf{I}$ containing only this index in this case, and setting $\mathbf{l} = 0$ and $\mathbf{w} = 1$. The contacts were modeled as frictional point contacts with a friction coefficient of $\mu = 1$, resulting in the shown friction cones of $45°$. Since in this case the quality index is smooth at the resolution of the computed atlas, we set $d = 1$ in Algorithm 2, which corresponds to evaluating one point of each chart only, e.g. its center point. Algorithm 2 evaluated the whole atlas in about 10 seconds in this situation. Note that if the kinematic constraints of the hand were neglected, the optimal force-closed grasp would have the contact normals equi-distributed in the plane, i.e., with angles of $120°$ between them [42]. However, this configuration is not reachable in our case, because it does not satisfy the joint-assembly and contact constraints of the hand-object system considered. The example, thus, emphasizes the relevance of taking into account both the kinematic and contact constraints when optimizing a given grasp, as proposed in this paper.

To illustrate a case where the quality index exhibits multiple local optima over $\mathcal{R}$, the same atlas was evaluated according to the normalized inverse condition number of the manipulability

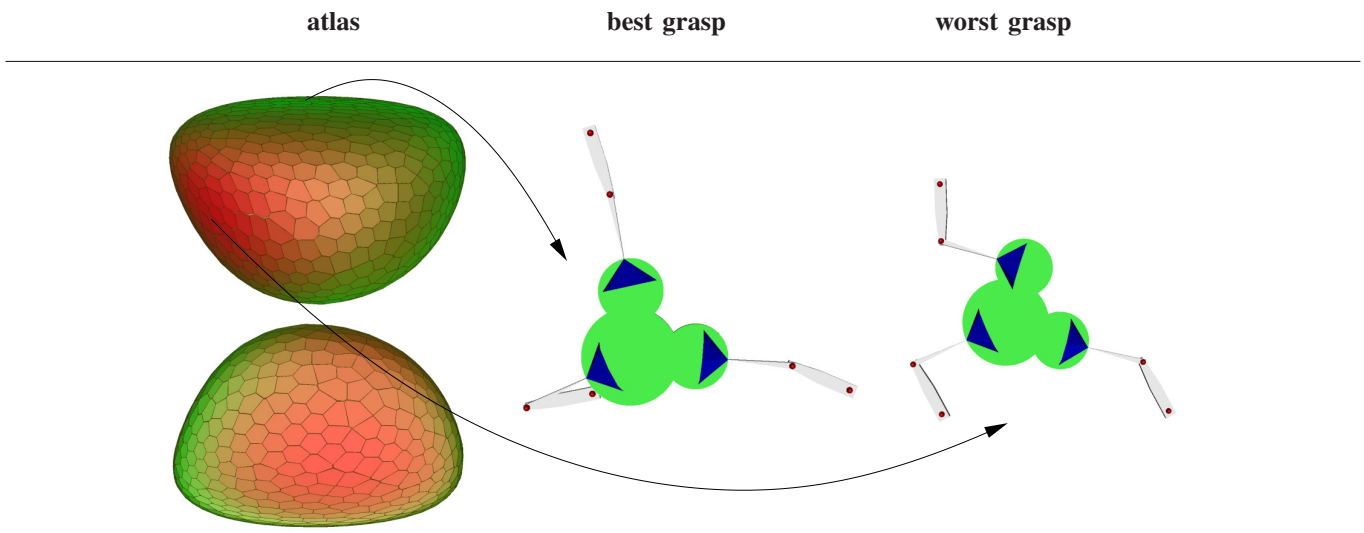

Fig. 8. Two views of the atlas of the set $\mathcal{R}$ of relevant grasps on the planar hand example, together with the best and worst grasp configurations obtained, according to the force-closure quality index in [2]. The views have been obtained by projecting the atlas on three of the problem variables. Green and red points in the views correspond to grasps with large and low values of the index, respectively.

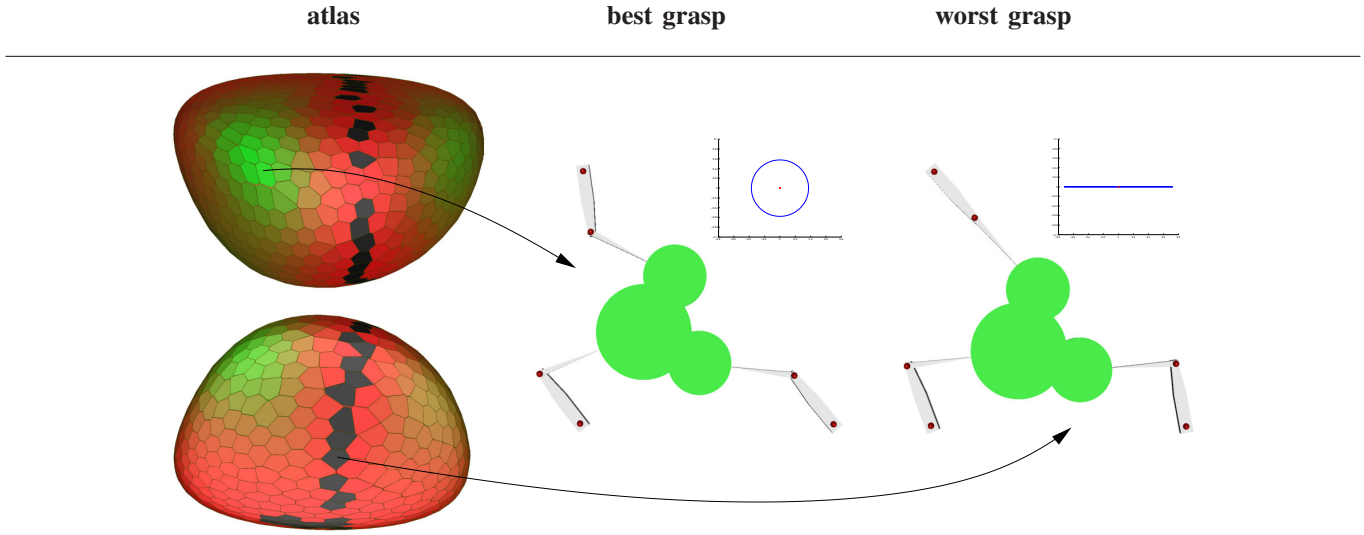

Fig. 9. The same views of the atlas in Fig. 8, but now colored according to the inverse of the condition number of the manipulability ellipsoid defined in [10]. Green and red points correspond to grasps with a large and low value of this index, respectively. Black corresponds to near-singular grasps. The atlas views show that this measure yields three local optimal grasps.

ellipsoid proposed by Bicchi and Prattichizzo [10], which is actually the ratio between the smallest and largest axis lengths of this ellipsoid. Algorithm 2 took 1.5 seconds in this case, and produced the results shown in Fig. 9, where the atlas views coincide with those in Fig. 8, but are now colored according to the new index. In the figure, green and red correspond to grasps with large and low values of this index, and black corresponds to grasps where the index is below 10^{-3}. In such near-singular grasps, the manipulability ellipsoid flattens in at least one direction, meaning that the hand can hardly move the object along that direction while maintaining the required contacts. Fig. 9 shows 2D projections of this ellipsoid revealing this fact, for the best and worst grasp configurations found. One of the fingers is fully extended in the worst configuration, which is in agreement with the inverse singularity condition of the 3-RRR parallel manipulator equivalent to this grasp [43]. Note from the figure that this quality index would pose difficulties to local optimization methods, since the index yields three local optimal grasps.

In a precision manipulation task, both the force-closure and the manipulability criteria may need to be taken into account. However, as it can be appreciated when comparing Figs. 8 and 9, these two criteria are conflicting in this example. The global optimum in Fig. 9, for example, corresponds to a point with a low value of the force closure index in Fig. 8. We use a serial evaluation approach, and optimize the manipulability index only for those grasps with a minimum value of the force-closure index. Fig. 10 shows the result of such strategy, obtained by applying Algorithm 2 with $\mathbf{I}= (I_1, I_2)^\top$, where I_1 and I_2 are the force-closure index and the inverse condition number of the manipulability ellipsoid, respectively, and using $\mathbf{l} = (0.2, 0)^\top$ and $\mathbf{w} = (0, 1)^\top$. These thresholds are set so that

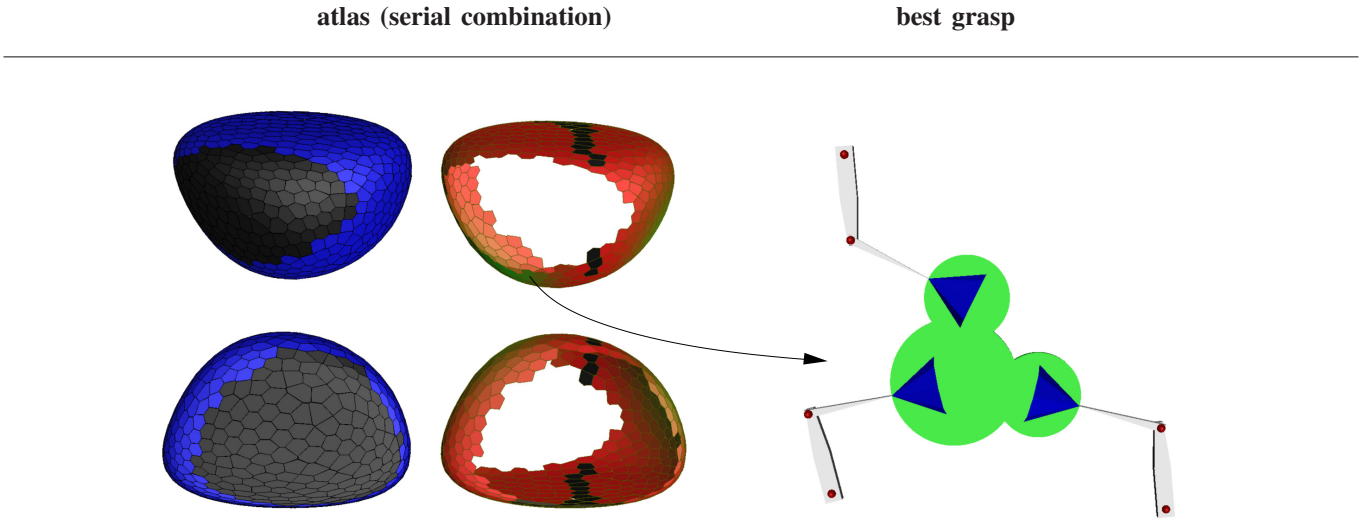

Fig. 10. The same views of the atlas in Figs. 8 and 9, but now evaluated under a serial approach that combines the force-closure and manipulability indices. The regions with a force-closure index above 0.2 are indicated in blue in the atlas. These regions are then evaluated according to the same manipulability index used in Fig. 9 to select the best configuration on them.

about half of the charts are discarded using the force-closure index. Clearly, the optimal grasp would be different if the indices were considered in the reverse order or with different thresholds.

B. The Schunk anthropomorphic hand

To validate the approach on a complex grasping device, we have applied it to the Schunk Anthropomorphic hand. Assuming that all joints are independently actuated, this hand has 13 degrees of freedom and, formulated according to [8], Eq. (1) is a system of 88 equations in 101 variables. The tests are performed using three objects: (1) a can, (2) a jeweler's screwdriver, and (3) a Marquina oil bottle. In all cases the grasps are to be performed using three fingers, and the complexity of the examples is determined by the dimension and the distribution of the contact regions.

In the case of the can, the contact regions at the fingertips are points. Moreover, the contact patch on the object for the thumb is reduced to a line along the can to avoid repeated solutions caused by the axial symmetry of the can, but the two other fingers are allowed to contact an identical cylindrical patch defined all over the surface of the can. Despite involving only one contact patch, its large extension makes this test case a hard one, because a large atlas will have to be computed. In the case of the screwdriver, a point on the index fingertip is set to be in contact with the flat head (to be able to apply forces that ensure a proper contact of the screwdriver with the screw), a point on the thumb is limited to move on a line along the screwdriver's body (to avoid symmetric solutions), and a curve on one side of the last phalanx of the third finger is constrained to contact the screwdriver's body at any point. Thus, this example illustrates the applicability of the method under different contact models. Finally, to properly dispense oil with the Marquina oil bottle, a point on the index finger must contact the top of the bottle along a curve, and points on the two other fingers must touch patches in the middle and bottom sections of the bottle, respectively. Therefore, the fingers contact the object on three disjoint regions with different sizes and orientations, which represents a general situation for the proposed approach.

After the contact constraints are imposed, Eq. (9) involves $f = 128$ equations in $n = 136$ variables (and hence $t = n - f = 8$) in the first example, $f = 131$ equations in $n = 141$ variables (and hence $t = 10$) in the second case, and $f = 133$ equations in $n = 142$ variables (and hence $t = 9$) in the third example. Thus, in order to obtain a set $\mathcal{R}$ of dimension $k = 2$, s must be set to 6, 8, and 7, respectively. Keeping at least 5 principal hand motions out of 13, we still retain more than 99% of the motion capability of the hand captured in the set $\mathbf{X}_{\mathrm{h}}$, which in this test case includes a database of human hand configurations adapted to the kinematics of the Schunk hand [37]. Previous approaches like [23] use less principal hand motions (typically 2), with the consequent decrease in motion capability of the hand. The atlases for the three examples were obtained in 170, 180, and 18 seconds using Algorithm 1 with $r = 1$ and $\epsilon = 0.5$, and they include 4900, 4800, and 400 charts, respectively. These times agree with the fact that the stronger the contact constraints, the less the number of charts in the atlas, and thus, the faster the generation of such atlas.

Fig. 11 shows the results of applying Algorithm 2 with $d = 1$ on the atlases obtained on the three examples, using the force-closure quality index in [2] with the same friction coefficient $\mu = 1$ used in the planar hand example. In this case, the spatial friction cones are linearly approximated using eight generators. The optimization for the three examples took 115, 120, and 9 seconds, respectively. These times basically scale with the number of charts in the atlas, and they are relatively large because the implementation of Algorithm 2 is in Matlab, and a linear program has to be solved for each grasp.

In the oil bottle test case, we also used $k = 3$, simply by considering one additional principal hand motion. In this

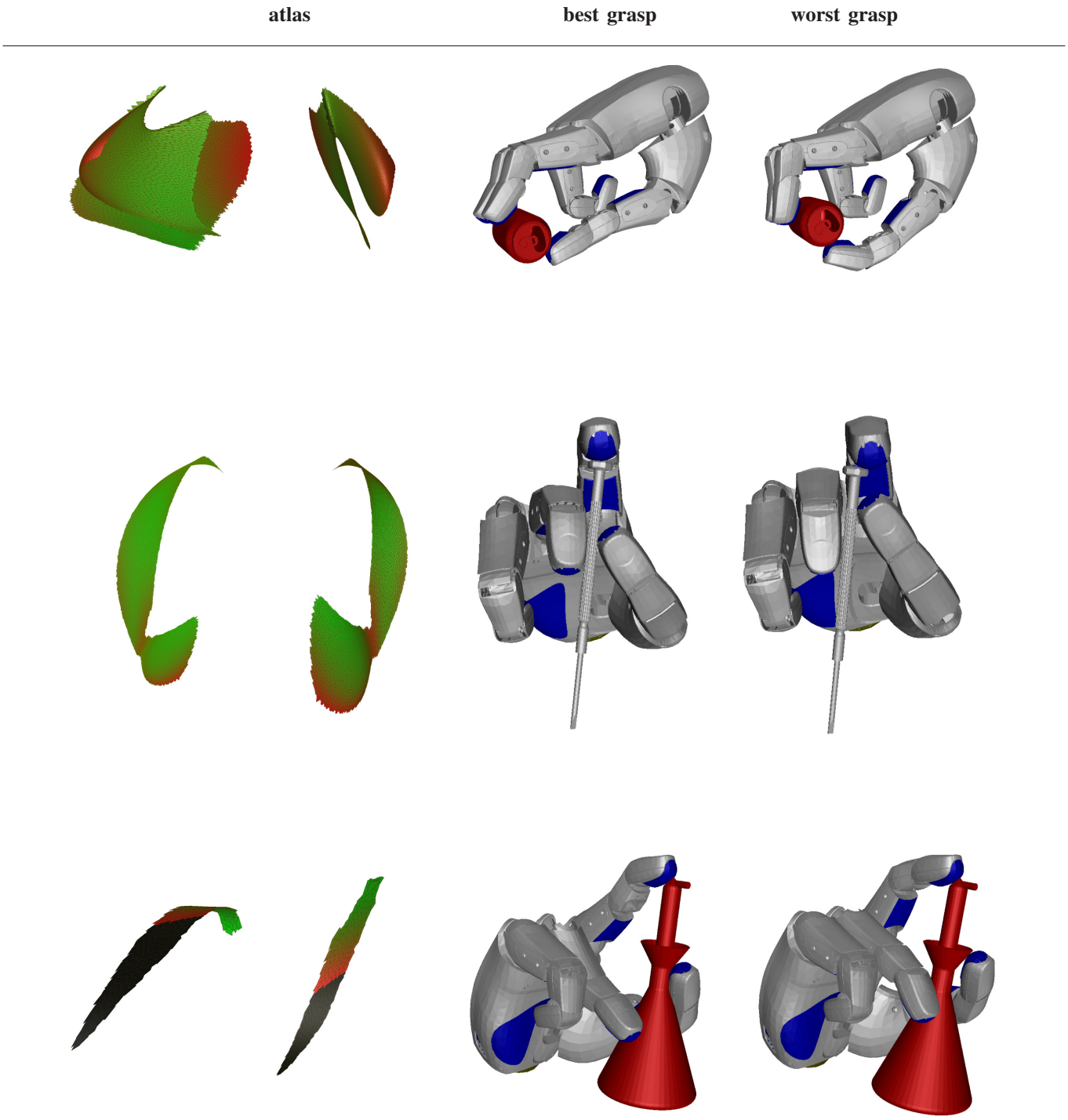

Fig. 11. Optimization of the force-closure quality index described in [2] for the Schunk anthropomorphic hand grasping a can (top), a jewelry screwdriver (middle), and an oil drizzler (bottom), assuming point contacts with a friction coefficient of $\mu = 1$. Two views of the atlas of the set $\mathcal{R}$ obtained for each object are shown, where green and red points correspond to configurations with large and small values of the index, respectively, and black points correspond to non-force-closed grasps. As in Figs. 8 to 10, the atlas views have been obtained by projection on three of the problem variables.

case, the atlas includes 12800 charts and the optimization takes 1050 seconds. However, the optimal grasp returned is almost the same as that obtained with $k = 2$, which confirms that, in this example, 6 principal hand motions are enough to capture most of the mobility of the hand.

Finally, we use the screwdriver example to optimize the grasp combining the force-closure and manipulability indices in parallel. This is achieved by normalizing the force-closure and the manipulability criteria and using $\mathbf{l} = (-\infty, -\infty)^\top$ and $\mathbf{w} = (0.6, 0.4)^\top$ in Algorithm 2, obtaining the grasp shown in Fig. 12. The combination exhibits different local maxima, but with the procedure introduced in this paper the global one is readily determined while a local optimizer might get stuck in a local extreme, depending on the initialization.

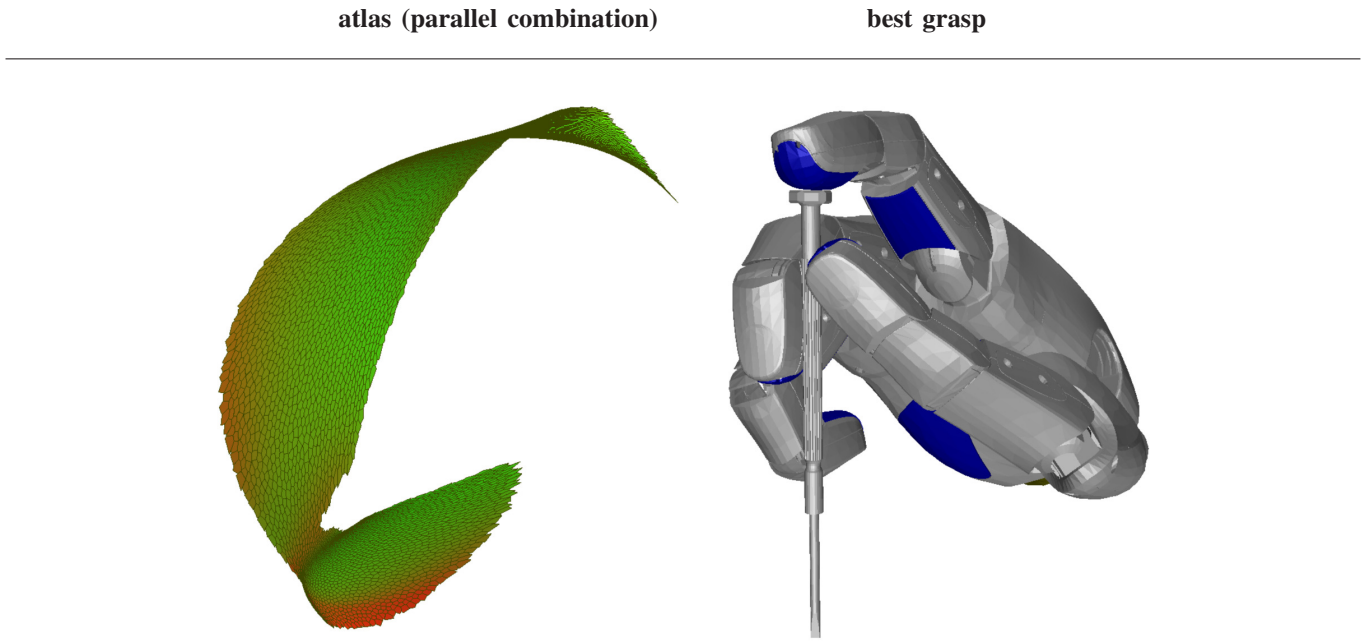

Fig. 12. The best grasp found when optimizing a weighted combination of the force closure and the manipulability criterion, where green and red, respectively correspond to grasps with a large and low value of this index.

VI. Conclusions

The work in this paper is part of a pipeline initiated in [8], for robotic grasp planning under specific contact constraints. The grasp synthesis method in [8] is herein extended with a procedure for optimizing the quality of the obtained grasps. The procedure enforces the satisfaction of all kinematic and contact constraints of the hand-object system during the optimization process, and it is global, in the sense that it explores the whole set of relevant grasps attainable from a given point, determining the optimal grasp at the selected resolution without getting trapped into local extrema. Moreover, the method is general, meaning that it can be applied to any hand/object geometry, and to any desired set of quality indices. The efficiency of the method critically depends on the dimension of the traced manifold. In the case of grasps, however, principal hand motions allow reducing the dimension of such manifold considerably. Actually, the proposed method keeps a large number of principal hand motions (up to 7 out of 13 for the Schunk hand), while previous methods [23, 36, 37] use a smaller number of them. This is because the procedure proposed here integrates the contact constraints a priori, which already introduces a large reduction in the problem dimension.

The grasping pipeline envisaged should include a module to actually execute the computed grasp. This requires to take into account dynamics, control, and path planning issues. To this end, the pipeline is being extended using impedance control techniques based on a kinestatic analysis of the grasp [44], and with a planner to compute an approach path to the object to be grasped [37]. Also, an analysis of the uncertainty would be necessary to achieve a successful execution of the grasp. Usually, the uncertainty analysis on manifolds is performed in the associated tangent bundle [45] and, thus, the atlas computed by the method could be of great help to this end. This point certainly deserves future attention.

The presented method operates in the connected component of the manifold of relevant grasps that are reachable from a given point. If the manifold has other connected components, the best grasp might be in any of the non-explored components. This is not an issue in most robotic hands since, due to joint-range limitations, the set of feasible grasps only contains one connected component usually. For the sake of generality, however, ways of obtaining one starting point in each component of the relevant grasp manifold should certainly be investigated.

Acknowledgments

The authors would like to thank Michael E. Henderson and O. Bohigas for fruitful discussions on the continuation method, and Patrick Grosch for providing 3D models for the test cases.

References

[1] K. B. Shimoga, "Robot grasp synthesis algorithms: A survey," *The International Journal of Robotic Research*, vol. 15, no. 3, pp. 230–266, 1996.

[2] D. Prattichizzo and J. C. Trinkle, "Grasping," in *Springer Handbook of Robotics*, B. Siciliano and O. Khatib, Eds. Springer Berlin Heidelberg, 2008, ch. 28, pp. 671–700.

[3] A. Sahbani, S. El-Khoury, and P. Bidaud, "An overview of 3D object grasp synthesis algorithms," *Robotics and Autonomous Systems*, vol. 60, no. 3, pp. 326–336, 2012.

[4] C. Borst, M. Fischer, and G. Hirzinger, "Calculating hand configurations for precision and pinch grasps," in *IEEE/RSJ International Conference on Intelligent Robots and System*, 2002, pp. 1553–1559.

[5] Y. Guan and H. Zhang, "Kinematic feasibility analysis of 3-D multifingered grasps," *IEEE Transactions on Robotics and Automation*, vol. 19, no. 3, pp. 507–513, 2003.

[6] P. Gorce and N. Rezzoug, "Grasping posture learning with noisy sensing information for a large scale of multifingered robotic systems," *Journal of Robotic Systems*, vol. 22, no. 12, pp. 711–724, 2005.

[7] J. Rosell, X. Sierra, L. Palomo, and R. Suárez, "Finding grasping configurations of a dexterous hand and an industrial robot," in *International Conference on Robotics and Automation*, 2005, pp. 1178–1183.

[8] C. Rosales, L. Ros, J. M. Porta, and R. Suárez, "Synthesizing grasp configurations with specified contact regions," *The International Journal of Robotics Research*, vol. 30, no. 4, pp. 431–443, 2011.

[9] C. Ferrari and J. Canny, "Planning optimal grasps," in *IEEE International Conference on Robotics and Automation*, 1992, pp. 2290–2295.

[10] A. Bicchi and D. Prattichizzo, "Manipulability of cooperating robots with unactuated joints and closed-chain mechanisms," *IEEE Transactions on Robotics and Automation*, vol. 16, no. 4, pp. 336–345, 2000.

[11] Y. Yokokohji, J. San Martin, and M. Fujiwara, "Dynamic manipulability of multifingered grasping," *IEEE Transactions on Robotics*, vol. 25, no. 4, pp. 947–954, 2009.

[12] Z. Li and S. Sastry, "Task-oriented optimal grasping by multifingered robot hands," *IEEE Transactions of Robotics and Automation*, vol. 4, no. 1, pp. 32–44, 1988.

[13] R. Haschke, J. J.Steil, I. Steuwer, and H. Ritter, "Task-oriented quality measures for dextrous grasping," in *International Symposium on Computational Intelligence in Robotics and Automation*, 2005, pp. 689–694.

[14] J. K. Salisbury and B. Roth, "Kinematics and force analysis of articulated mechanical hands," *Journal of Mechanisms, Transmissions and Actuation in Design*, vol. 105, no. 1, pp. 35–41, 1983.

[15] B. Mishra, J. T. Schwartz, and M. Sharir, "On the existence and synthesis of multifinger positive grips," *Algorithmica*, vol. 2, no. 4, pp. 541–558, 1987.

[16] Z. Ji and B. Roth, "Contact force in grasping and kinematic constraints," in *Seventh IFToMM World Congress*, 1987, pp. 1219–1222.

[17] V.-D. Nguyen, "Constructing force-closure grasps," *The International Journal of Robotics Research*, vol. 7, no. 3, pp. 3–16, 1988.

[18] J. C. Trinkle, A. O. Farahat, and P. F. Stiller, "First-order stability cells of active multi-rigid-body systems," *IEEE Transactions on Robotics and Automation*, vol. 11, no. 4, pp. 545–557, 1995.

[19] Y.-H. Liu, "Computing n-finger form-closure grasps on polygonal objects," *The International Journal of Robotics Research*, vol. 19, no. 2, pp. 149–158, 2000.

[20] N. S. Pollard, "Closure and quality equivalence for efficient synthesis of grasps from examples," *The International Journal of Robotics Research*, vol. 23, no. 6, pp. 595–613, 2004.

[21] X. Zhu and H. Ding, "An efficient algorithm for grasp synthesis and fixture layout design in discrete domain," *IEEE Transactions on Robotics*, vol. 23, no. 1, pp. 157–163, 2007.

[22] M. Roa and R. Suárez, "Computation of independent contact regions for grasping 3-D objects," *IEEE Transactions on Robotics*, vol. 25, no. 4, pp. 839–850, 2009.

[23] M. T. Ciocarlie and P. K. Allen, "Hand posture subspaces for dexterous robotic grasping," *The International Journal of Robotics Research*, vol. 28, no. 7, pp. 851–867, 2009.

[24] M. Santello, M. Flanders, and J. F. Soechting, "Postural hand synergies for tool use," *The Journal of Neuroscience*, vol. 18, no. 23, pp. 10 105–10 115, 1998.

[25] J. A. Claret and R. Suárez, "Efficient and practical determination of grasping configurations for anthropomorphic hands," in *18th IFAC World Congress*, 2011, pp. 14 660–14 666.

[26] R. Platt, A. H. Fagg, and R. A. Grupen, "Null-space grasp control: theory and experiments," *IEEE Transactions on Robotics*, vol. 26, pp. 282–295, 2010.

[27] G. Liu, J. Xu, X. Wang, and Z. Li, "On quality functions for grasp synthesis, fixture planning, and coordinated manipulation," *IEEE Transactions on Automation Science and Engineering*, vol. 1, no. 2, pp. 146–162, 2004.

[28] S. K. Song, J. B. Park, and Y. H. Choi, "Dual-Fingered stable grasping control for an optimal force angle," *IEEE Transactions on Robotics*, vol. 28, no. 1, pp. 256–262, 2012.

[29] M. E. Henderson, *Numerical continuation methods for dynamical systems: path following and boundary value problems*. Springer, 2007, ch. Higher-Dimensional Continuation.

[30] C. Rosales, J. M. Porta, and L. Ros, "Global optimization of robotic grasps," in *Robotics: Science and Systems*, 2011, pp. 289–296.

[31] L. Birglen, C. Gosselin, and T. Laliberté, *Underactuated robotic hands*, ser. Tracks in Advanced Robotics. Springer Verlag, 2008, vol. 40.

[32] J. Denavit and R. Hartenberg, "A kinematic notation for lower-pair mechanisms based on matrices," *Transactions of the ASME. Journal of Applied Mechanics*, vol. 23, pp. 215–221, 1955.

[33] J. M. Porta, L. Ros, and F. Thomas, "A linear relaxation technique for the position analysis of multiloop linkages," *IEEE Transactions on Robotics*, vol. 25, no. 2, pp. 225–239, 2009.

[34] C. Wampler and A. Morgan, "Solving the 6R inverse position problem using a generic-case solution methodology," *Mechanism and Machine Theory*, vol. 26, no. 1, pp. 91–106, 1991.

[35] G. Farin, *Curves and Surfaces for CAGD: A Practical Guide*, 5th ed. Morgan Kaufmann, November 2001.

[36] A. Bicchi, M. Gabiccini, and M. Santello, "Modeling natural and artificial hands with synergies," *Philosophical Transactions of the Royal Society B*, vol. 366, pp. 3153–3161, 2011.

[37] J. Rosell, R. Suárez, C. Rosales, and A. Pérez, "Autonomous motion planning of a hand-arm robotic system based on captured human-like hand postures," *Autonomous Robots*, vol. 31, no. 1, pp. 87–102, 2011.

[38] M. E. Henderson, "Multiparameter parallel search branch switching," *International Journal of Bifurcation and Chaos in Applied Science and Engineering*, vol. 15, no. 3, pp. 967–974, 2005.

[39] ——, "Multiple parameter continuation: Computing implicitly defined k-manifolds," *International Journal of Bifurcation and Chaos*, vol. 12, no. 3, pp. 451–476, 2002.

[40] R. Suárez, M. Roa, and J. Cornellà, "Grasp quality measures," Institut d'Organització i Control de Sistemes Industrial, UPC, Tech. Rep. IOC-DT-P-2006-10, 2006.

[41] The CUIK project, http://www.iri.upc.edu/cuik.

[42] B. Mirtich and J. Canny, "Easily computable optimum grasps in 2-D and 3-D," in *IEEE International Conference on Robotics and Automation*, 2002, pp. 739–747 vol.1.

[43] I. Bonev, D. Zlatanov, and C. Gosselin, "Singularity analysis of 3-DOF planar parallel mechanisms via screw theory," *ASME Journal of Mechanical Design*, vol. 125, pp. 573–581, 2003.

[44] C. Rosales, R. Suárez, M. Gabiccini, and A. Bicchi, "On the synthesis of feasible and prehensile robotic grasps," in *IEEE international conference on Robotics and Automation*, 2012, pp. 550–556.

[45] G. S. Chirikjian, *Stochastic Models, Information Theory, and Lie Groups, Volume 1: Classical Results and Geometric Methods*. Birkhäuser, 2009.

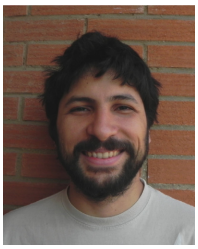

Carlos Rosales received the Mechanical Engineering degree from the Universidad de Carabobo, Venezuela, in 2003, a master in Mechatronics from the Universitat Politècnica de Catalunya (UPC), Spain, in 2006, and the PhD degree (with honors) in Robotics and Advanced Automation from the UPC in 2013. In 2011 he was a visiting scholar at the Research Center "E. Piaggio" of the University of Pisa. His main research topic is the consideration of kinematic and static limitations for grasp synthesis. He is also interested in motion planning and geometric methods in robot position analysis.

Josep M. Porta received the Engineering degree in Computer Science in 1994, and the Ph.D. degree (with honors) in Artificial Intelligence in 2001, both from the Universitat Politècnica de Catalunya, Spain. From 2001 to 2003 he held a postdoctoral position at the University of Amsterdam, doing research in autonomous robot localization using vision. Currently, he is an Associate Researcher of the Spanish National Research Council at the Institut de Robòtica i Informàtica Industrial (IRI, CSIC-UPC), Barcelona, Spain. His current research interests include planning under uncertainty and computational kinematics.

Lluís Ros received the Mechanical Engineering degree in 1992, and the Ph.D. degree (with honors) in Robotics and Automation in 2000, both from the Universitat Politècnica de Catalunya (UPC). From 1993 to 1996 he worked with the Control Division of the Institut de Cibernètica (Barcelona). He was a visiting scholar at York University (Toronto, 1997), University of Tokyo (Tokyo, 1998), and the Laboratoire d'Analyse et Architecture des Systèmes (Toulouse, 1999). He joined the Institut de Robòtica i Informàtica Industrial (IRI, CSIC-UPC) in 1997, where he is an Associate Researcher of the Spanish National Research Council (CSIC) since 2004. His research interests include geometry and kinematics, with applications to robotics, computer graphics, and machine vision.